Covalent Bonding Aptamer with Enhanced SARS-CoV-2 RBD-ACE2 Blocking and Pseudovirus Neutralization Activities

Zichen Qin, Yiying Zhu and Yu Xiang*

Department of Chemistry, Key Laboratory of Bioorganic Phosphorus Chemistry and Chemical Biology (Ministry of Education), Beijing Key Laboratory for Microanalytical Methods and Instrumentation, Tsinghua University, Beijing 100084, China.

*Email: xiang-yu@tsinghua.edu.cn

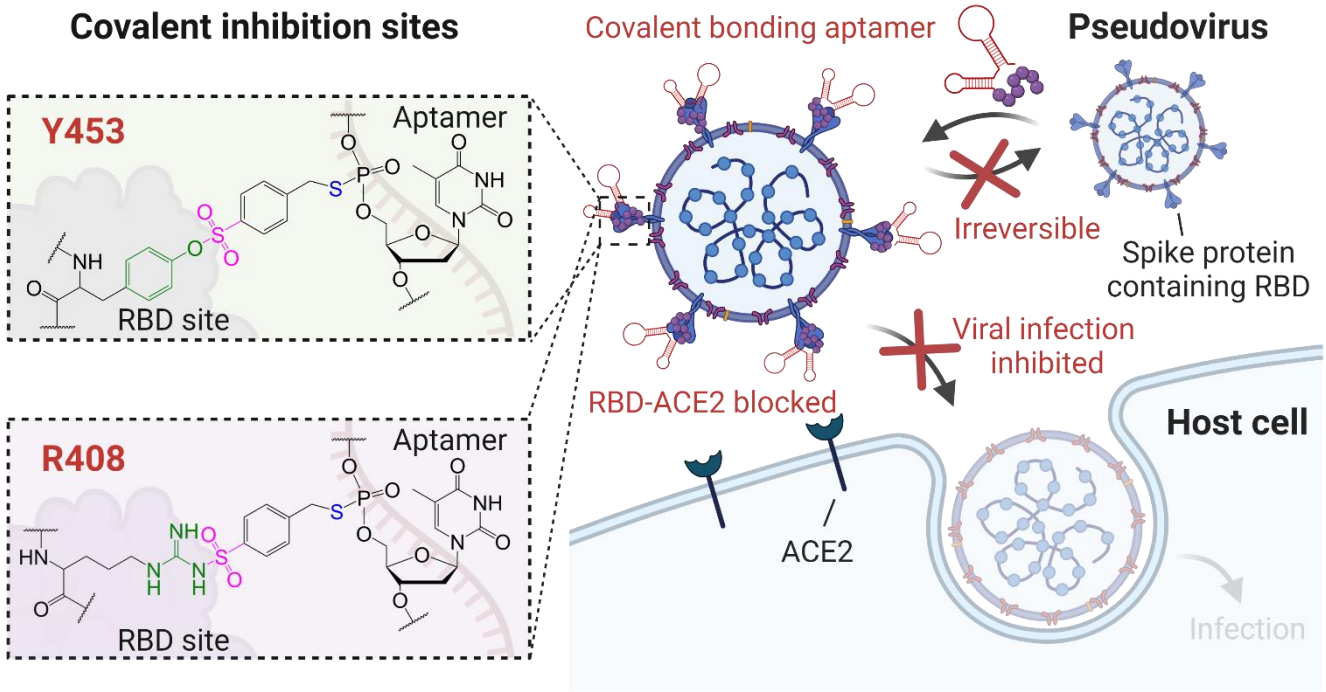

A chemically modified RBD aptamer containing sulfur(VI) fluoride exchange (SuFEx) modifications blocks the RBD-ACE2 interaction through a covalent bonding mechanism at the RBD-ACE2 binding interface, showing more than 25-fold enhancement of SARS-CoV-2 pseudovirus neutralization efficacy over the original aptamer.

Covalent Bonding Aptamer with Enhanced SARS-CoV-2 RBD-ACE2 Blocking and Pseudovirus Neutralization Activities

Zichen Qin, Yiying Zhu and Yu Xiang*

Department of Chemistry, Key Laboratory of Bioorganic Phosphorus Chemistry and Chemical Biology (Ministry of Education), Beijing Key Laboratory for Microanalytical Methods and Instrumentation, Tsinghua University, Beijing 100084, China.

*Email: xiang-yu@tsinghua.edu.cn

Supporting Information is provided as a separated file with this manuscript.

Abstract

SARS-CoV-2 uses its spike protein receptor-binding domain (RBD) to interact with the angiotensin-converting enzyme 2 (ACE2) receptor on host cells. Inhibitors of the RBD-ACE2 interaction are therefore promising drug candidates in treating COVID-19. Here, we report a covalent bonding aptamer that can block the RBD-ACE2 interaction and neutralize SARS-CoV-2 pseudovirus infection by forming covalent bonds on RBD, resulting in more than 25-fold enhancement of pseudovirus neutralization efficacy over the original binding aptamer. The chemically modified aptamer is equipped with sulfur(VI) fluoride exchange (SuFEx) modifications and covalently targets important RBD residues within the RBD-ACE2 binding interface, including Y453 and R408. The covalent bonding is highly specific to RBD over other proteins such as human serum albumin (HSA), ACE2 and immunoglobulin G1 (IgG1) Fc. Our study demonstrates the promise of introducing covalent inhibition mechanisms for developing robust RBD-ACE2 inhibitors against SARS-CoV-2 infection.

Introduction

SARS-CoV-2 infection is initiated by the recognition between the SARS-CoV-2 spike protein receptor-binding domain (RBD) and the host cell receptor angiotensin-converting enzyme 2 (ACE2).[1-2] For this reason, many promising inhibitors target the RBD-ACE2 protein-protein interaction (PPI) for potential treatment of COVID-19, including antibodies,[3-4] small molecules,[5-6] peptides[7-8] and DNA aptamers.[9-15] All the currently known RBD-ACE2 inhibitors act through noncovalent binding with RBD or ACE2 to block the SARS-CoV-2 entry into host cells. Due to the strong RBD-ACE2 interaction in nature,[1-2] these reversible inhibitors must be competitive in the binding equilibrium, and usually their multimerization[9-15] into large molecules is required for higher inhibition efficacy. On the other hand, covalent inhibitors, whose mechanism involves irreversible chemical bond formation between the inhibitors and their target proteins, offer advantages including higher potency and longer duration of inhibition.[16-19] As another strategy beyond multimerization, the covalent inhibition mechanism can enhance RBD-ACE2 blocking and provide more robust inhibitors. Despite of the promise, no covalent RBD-ACE2 inhibitor is reported so far.

Substantial success has been achieved in developing small molecule covalent drugs as enzyme inhibitors,[20-21] including those directing towards the active sites of kinases and proteases[22-24] through cysteine-[25] and lysine-targeting[26] warheads. However, to target PPIs of interest, small molecules are generally inefficient in binding shallow protein surfaces or competing with PPI spanning a large binding interface at the thousand square angstrom level. Thus, it is extremely difficult to develop small molecule covalent inhibitors against PPIs.[27] Instead, biomolecules, such as peptides[28-29] and proteins[30-31] are more suitable candidates to covalently inhibit PPIs. In addition, to ensure both selectivity and efficacy of inhibitors in covalent bonding at or near the PPI interface, a latent warhead is needed to stay weakly nucleophilic in the complicated biological environment until binding and reacting with the context-specific target amino acid residues. Warheads based on the sulfur(VI) fluoride exchange (SuFEx) chemistry[32-35] meet the criteria very well.

Despite that proteins,[3-4] peptides,[7-8] and DNA aptamers[9-15] have been identified to bind the SARS-CoV-2 RBD and spike protein, constructing covalent inhibitors of RBD-ACE2 based on these biomolecules is nontrivial. No free cysteine is available on RBD at or near the RBD-ACE2 binding interface, so that the widely used cysteine-targeting strategy is not effective.[36] Taking advantage of the well-established crystal structure of thrombin-aptamer complex, covalent bonding aptamers with sulfonyl fluoride[37] and sulfonamide[38] warheads were recently developed by rational designs to target thrombin. Unfortunately, no structure of RBD-aptamer complex is currently available, and RBD-ACE2 as a PPI is much more difficult to inhibit covalently than thrombin as an enzyme with active sites.

To address the challenge, in this work, we developed a covalent bonding aptamer against RBD-ACE2 by equipping an RBD aptamer with SuFEx modifications. This chemically modified aptamer inhibited RBD-ACE2 via a covalent bonding mechanism and showed enhanced activities in both SARS-CoV-2 RBD-ACE2 blocking and pseudovirus neutralization over the original aptamer.

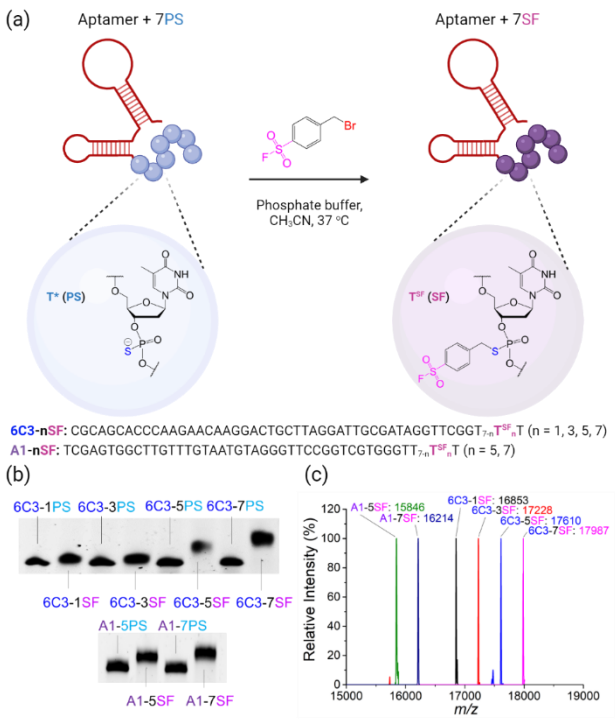

Figure 1. (a) Synthesis of covalent bonding aptamers, where the asterisks indicate PS sites for SuFEx modifications. (b) Denatured PAGE images of PS-aptamers before and after SF modifications. (c) ESI-MS analyses of SF-modified aptamers. Calculated/detected *m/z*: 6C3-1SF (16855/16853), 6C3-3SF (17231/17228), 6C3-5SF (17607/17610), 6C3-7SF (17983/17987), A1-5SF (15841/15846), A1-7SF (16217/16214).

Results and Discussion

We chose to modify the two known RBD aptamers, named 6C3[9] and A1,[10] which were reported to bind RBD with dissociation constants of about 45 and 28 nM, respectively, to show the generality of our method to convert original binding aptamers into covalent bonding ones. We utilized an efficient reaction between 4-(bromomethyl)benzenesulfonyl fluoride (Br-SF) and phosphorothioate (PS) under a mild condition to introduce multiple SuFEx modifications (Figure 1a), similar to our previous works on modifying DNA[39] and RNA[40] with redox-responsive groups. Without any structure of RBD-aptamer complex in hand, we carried out a tail modification strategy and attached an eight-thymidine (8T) fragment containing one or multiple PS modifications to the 3′ end of the aptamers (Figure 1a). We successfully incorporated 1, 3, 5, or 7 sulfonyl fluoride (SF) modifications to the 3′ end 8T on 6C3, as well as 5 or 7 SF to that of A1, as confirmed by the denatured polyacrylamide gel electrophoresis (PAGE, Figure 1b) and electrospray ionization-mass spectrometry (ESI-MS, Figure 1c) analyses.

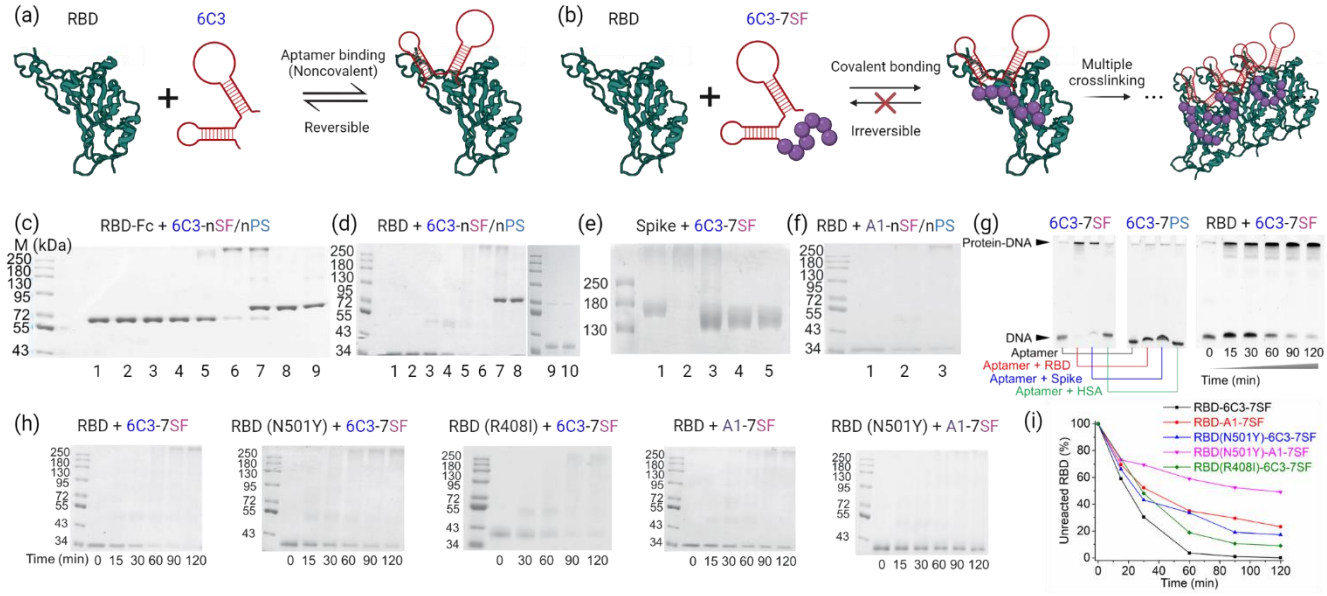

Figure 2. (a) Reversible binding between 6C3 and RBD. (b) Irreversible covalent bonding between 6C3-7SF and RBD. (c) SDS-PAGE of Fc-tag RBD reacted with 6C3 w/wo SuFEx. Lane 1~9: RBD-Fc; RBD-Fc+6C3-7PS; RBD-Fc+6C3-1SF; RBD-Fc+6C3-3SF; RBD-Fc+6C3-5SF; RBD-Fc+6C3-7SF; RBD-Fc+6C3-7SF+HSA; HSA; 6C3-7SF+HSA. (d) SDS-PAGE of His-tag RBD reacted with 6C3 w/wo SuFEx. Lane 1~10: RBD; RBD+6C3-7PS; RBD+6C3-1SF; RBD+6C3-3SF; RBD+6C3-5SF; RBD+6C3-7SF; RBD+6C3-7SF+HSA; 6C3-7SF+HSA; IgG1 Fc; 6C3-7SF+IgG1 Fc. (e) SDS-PAGE of spike protein reacted with 6C3-7SF. Lane 1~5: Spike; Spike+6C3-7SF; Spike+6C3-7SF+ACE2; ACE2; 6C3-7SF+ACE2. (f) SDS-PAGE of His-tag RBD reacted with A1 w/wo SuFEx. Lane 1~3: RBD; RBD+A1-5SF; RBD+A1-7SF. (g) Denatured PAGE of 6C3-7SF and 6C3-7PS reacted with proteins. (h) Kinetics of the covalent bonding between RBD variants and SF-modified aptamers. (i) Data chart of the covalent bonding kinetics from (h). For all the above reactions, 1 μM RBD and 1.5 μM aptamers (except for 1 μM aptamers in (g)) were reacted for 2 h or the indicated time in 1×phosphate buffer saline (PBS, pH 7.4) containing 2 mM $MgCl_2$.

Different from the traditional aptamer binding mode (Figure 2a), we observed efficient covalent bonding (Figure 2b) between RBD and SF-modified 6C3 aptamers containing 5 or 7 SF modifications, regardless of using Fc-tag or His-tag RBD proteins, as illustrated in the sodium dodecyl sulfate-polyacrylamide gel electrophoresis (SDS-PAGE) analyses (Figure 2c and 2d). The 6C3 aptamers with none, 1, or 3 SF conferred little reaction under the same condition, indicating the critical role of more SF modifications. The cross-linked adducts of large molecular weights (> 250 kDa) were formed between RBD and the covalent bonding aptamers, which was not surprising considering that multiple potential reactive groups were on both RBD and SF-modified aptamers. The GH_6 His tag peptide did not react with 6C3-7SF (Figure S1a, Supporting Information), excluding the possibility of His tag reactivity. The SARS-CoV-2 spike protein (Spike) containing RBD was

found active in covalent bonding with 6C3-7SF as well (Figure 2e). The covalent reaction between 6C3-7SF and RBD/Spike was highly selective over human serum albumin (HSA), ACE2 (Fc tag) and immunoglobulin G1 (IgG1) Fc as shown in Figure 2c and 2d, and occurred efficiently in diluted human serum (Figure S1b). Interestingly, a shortened version of 6C3-7SF maintained the covalent bonding reactivity and selectivity to RBD (Figure S1c and S1d), suggesting the covalent bonding aptamer did not require the full and strong binding affinity for the high bonding reactivity and selectivity. Two non-aptamer oligonucleotides with 7 SF modifications were inactive with RBD (Figure S2), indicating the essential role of the aptamer recognition. A1 aptamers equipped with 5 or 7 SF also showed covalent bonding activities to RBD (Figure 2f), indicating the generality of our method to construct covalent bonding aptamers. In addition to SDS-PAGE, denatured PAGE visualizing the DNA components also supported the successful covalent bonding between 6C3-7SF and RBD (Figure 2g), where protein-DNA adducts were too large to migrate efficiently without SDS so they accumulated at the top of the gels. Monitoring the kinetics of covalent bonding between 6C3-7SF and the RBD variants gave reaction half time ($t_{1/2}$) values around half an hour (Figure 2h and 2i) for each of the proteins, with mutants N501Y and R408I reacting slower than the native RBD. Such rates were indeed comparable to the reported covalent aptamers for thrombin,[37-38] as well as the covalent peptides[28-29] and proteins[30-31] based on the SuFEx warheads. We also detected slower but still promising rates of covalent bond formation for A1-7SF with the RBD variants when compared with 6C3-7SF (Figure 2h and 2i), suggesting that a better dissociation constant (28 nM for A1 versus 45 nM for 6C3) of the original binder did not ensure a higher reactivity for the corresponding covalent bonder, probably due to the distinct RBD binding sites for each of the aptamers.

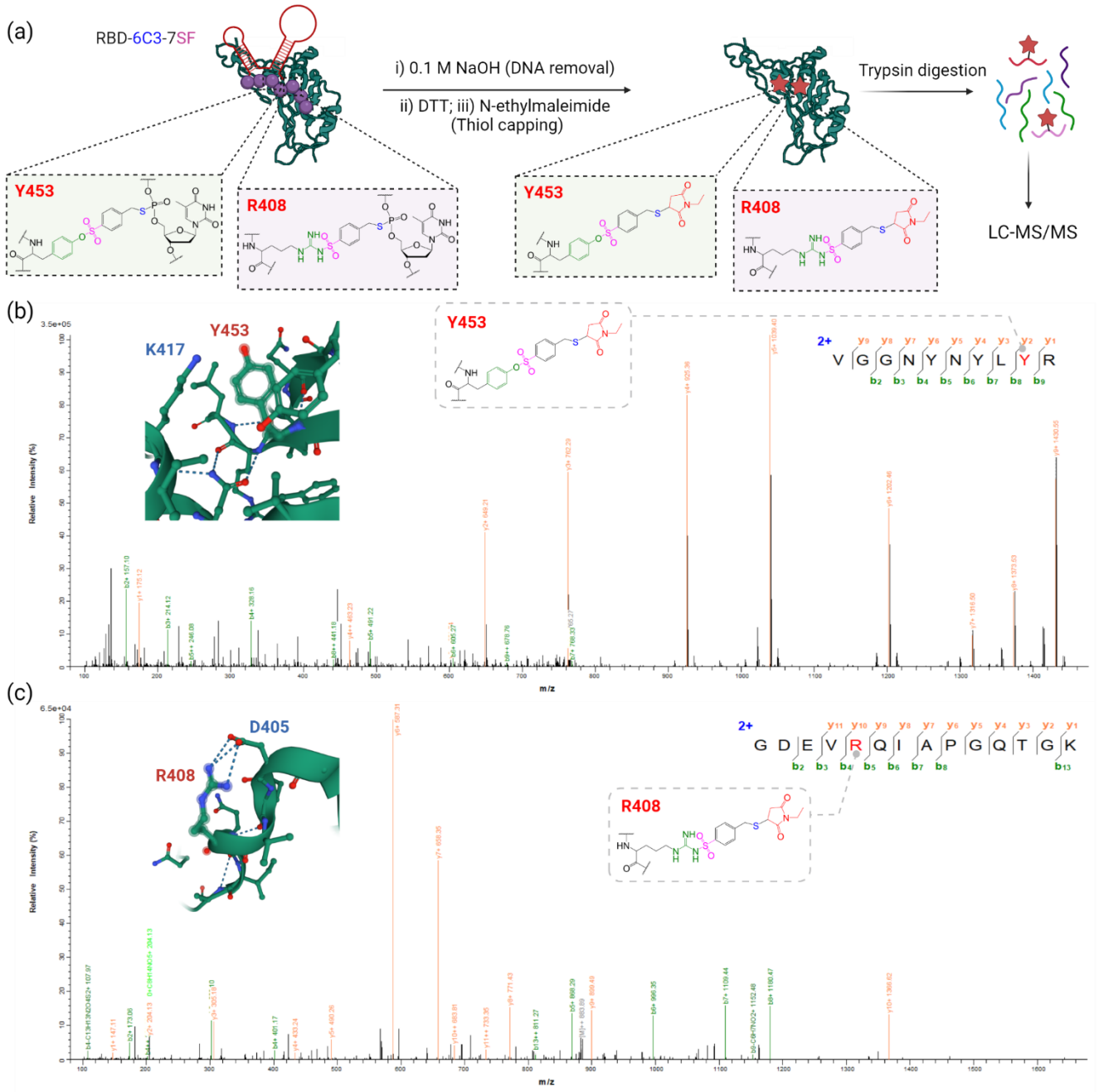

Figure 3. (a) Procedures for identifying covalent bonding sites in RBD-6C3-7SF adducts. (b)-(c) Peptide fragmentation MS/MS showing the modifications of Y453 (b) and R408 (c) in RBD-6C3-7SF adducts. The red tyrosine (Y) in (b) and arginine (R) in (c) are modified with the characteristic mark sulfonyl-CH_2-S-N-ethylmaleimide (SSNEM) and gives $\Delta m/z$ = y2−y1 = 474.09 (tyrosine−H_2O+SSNEM, calc. 474.09) in (b) and $\Delta m/z$ = y10−y9 = 467.13 and b5−b4 = 467.12 (arginine−H_2O+SSNEM, calc. 467.13) in (c). The insert folding structures in (b) and (c) are from Protein Data Bank 7EAZ and 7EB0, respectively.

We investigated the covalent bonding sites in RBD-6C3-7SF adducts by liquid chromatography coupled with tandem mass spectrometry (LC-MS/MS) analysis (Figure 3). DNA components were cleaved from RBD-6C3-7SF by 0.1 M NaOH treatment to hydrolyze the phosphorothioate esters, leaving thiol-containing sulfonyl marks on the proteins. These marks, along with RBD cysteines, were treated with the disulfide

reduction reagent DL-dithiothreitol (DTT) and then capped with N-ethylmaleimide. The proteins were then digested by trypsin and analyzed by LC-MS/MS (Figure 3a). By manual inspection of MS/MS spectra of interest generated by the Proteome Discoverer 2.4 software to confirm peptide sequences and modification sites with the characteristic mass addition, we identified six RBD residues as the possible bonding sites, including K378, R408, Y422, Y424, Y453 and K458 (Figure S3). Among them, Y453 (Figure 3b) and R408 (Figure 3c) are of particluar interest, because in the reported crystal structure of RBD-ACE2 complex,[1-2] RBD Y453 and R408 directly interact with the ACE2 H34 and N90 glycan, respectively. These two residues must be in some special context provided by the protein folding, so that they aquire sufficient reactivity with 6C3-7SF beyond the binding-induced proximity. The sterically adjacent K417 as a basic residue might enhance the reactivity of Y453 with the SuFEx warhead.[33] The nearby acidic D405 could form hydrogen bonds with R408 to activate the guanidinium, similar as the case of arginine methyltransferases.[41]. We were surprised by the reactivity of 6C3-7SF toward RBD R408, because no literature study identified any non-N-terminal arginine capable of reacting with SuFEx warheads. We repeated the analysis using another batch of RBD-6C3-7SF adducts and again identified R408 as the covalent bonding site in high confidcence (Figure S4). The faster reaction of 6C3-7SF with the native RBD than the R408I variant (Figure 2h and 2i) might also support the involvement of R408 in the covalent bonding sites. We did not observe the reactivity of 6C3-7SF toward the arginine-containing short peptide fragment (Figure S1a), suggesting the crucial role of protein-provided context for the R408 reactivity. We also detected RBD K378, Y422, Y424 and K458 as the other four possible covalent bonding sites (Figure S5-S8), which are within the RBD-ACE2 binding interface or responsible for protein folding. In comparison, using RBD to react with 5 mM *p*-toluenesulfonyl fluoride as a control, we were only able to detect and verify solely K458 (Figure S9), indicating a poor RBD reactivity without the aptamer recognition and binding-induced proximity. We did not detect any covalent bonding site when using RBD alone as the negative control. These results strongly support the potential of our covalent bonding

aptamer to block SARS-CoV-2 RBD-ACE2 and possibly neutralize the virus infection.

We utilized a commercially available enzyme-linked immunosorbent assay (ELISA) kit to assess the RBD-ACE2 blocking efficacy of the aptamers (Figure 4a).[42] The original 6C3 had only a weak inhibition activity even at 200 nM, and 1 SF modification was unable to provide apparent improvement (Figure 4a), in agreement with our SDS-PAGE results showing that 6C3 with 1 SF was insufficient for covalent bonding with RBD (Figure 2c and 2d). In contrast, dramatic enhancement of RBD-ACE2 blocking was observed for 200 nM 6C3-7SF (Figure 4a), demonstrating the advantage of endowing the covalent inhibition mechanism. By nonlinear fitting using the dose-response sigmoidal function, we detected the half-maximal inhibitory concentration (IC_{50}) as $IC_{50\ (RBD)}$ = 37.2 ± 2.4, $IC_{50\ (RBD\text{-}N501Y)}$ = 31.5 ± 11.5, and $IC_{50\ (RBD\text{-}R408I)}$ = 33.4 ± 3.1 nM for 6C3-7SF when blocking the variant RBD-ACE2 (Figure 4a). The similar IC_{50} values of 6C3-7SF (around 30 nM) to all the three RBD variants were likely because the diffusion of 6C3-7SF to the proteins on the plate surface became the rate-limiting factor for the covalent reactions (around 100 nM RBD used for ELISA plate coating). Nevertheless, the original binding aptamer 6C3 had IC_{50} well above the highest concentration used (200 nM) to the RBD variants (Figure 4a).

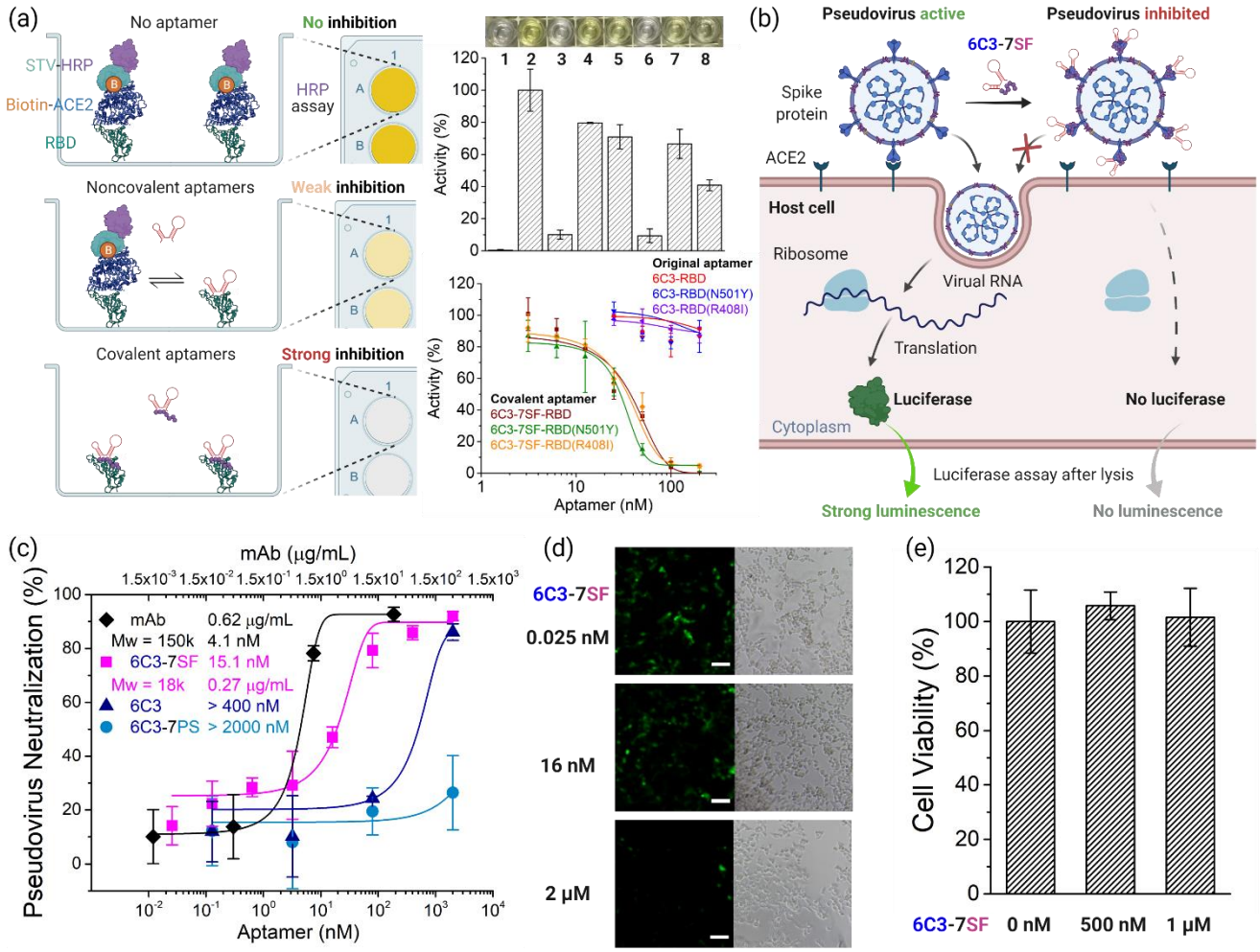

Figure 4. (a) ELISA assessing the RBD-ACE2 blocking activity of 6C3-7SF (STV: streptavidin, HRP: horseradish peroxidase), bar chart showing the RBD-ACE2 blocking efficiency of different aptamers (sample 1~8: no RBD as blank; no aptamer as negative control; positive control (500 nM inhibitor from the ELISA kit); 200 nM 6C3; 200 nM 6C3-1SF; 200 nM 6C3-7SF; 1 μM 6C3; 2 μM 6C3) (error bars are from n = 3), and RBD-ACE2 blocking activities of 6C3 w/wo 7SF against RBD, RBD-N501Y and RBD-R408I (error bars are from n = 3). (b) Principle of the SARS-CoV-2 pseudovirus neutralization activity assay based on infection-induced luciferase production in ACE2-expressing 293T cells. (c) Pseudovirus neutralization activities of a commercial monoclonal antibody (mAb), the aptamer 6C3-7SF, 6C3 and 6C3-7PS (error bars are from n = 3). (d) Fluorescence images of cells infected by pseudoviruses treated with 6C3-7SF at different concentrations. The scale bars are 100 μm. (e) Cytotoxicity of 6C3-7SF at different concentrations (error bars are from n = 6). In (c), (d) and (e), all aptamers used were double-end modified with Spacer 9 to enhance stability.

We also tested the pseudovirus neutralization activities of the covalent bonding aptamer. Inactivated HIV particles pseudotyped with SARS-CoV-2 spike proteins on surface and carrying green fluorescent protein (GFP) and luciferase reporter genes were used as the SARS-CoV-2 pseudoviruses (Figure 4b). They were mixed with serial dilutions of aptamers (all aptamers modified with Spacer 9, a 3-mer oligo-PEG, at both 5′

and 3′ ends to ensure stability, Table S1 and Figure S10) in Gibco Dulbecco's Modified Eagle Medium (DMEM) containing 10% fetal bovine serum (FBS) for 2.5 h, followed by incubation with 293T cells stably expressing human ACE2 for 6 h infection. After medium refresh, the cells were incubated for 48 h and then lysed for luciferase assays to estimate the neutralization efficacy (Figure 4c). We took a commercial monoclonal antibody as the positive control to validate our pseudovirus neutralization assay setup, with its IC_{50} detected as 0.62 ± 0.02 μg/mL versus the supplier provided value of 0.41 μg/mL. The IC_{50} values of noncovalent aptamers 6C3 and 6C3-7PS were found as > 400 nM and > 2000 nM to the pseudovirus, respectively, where the lower activity of 6C3-7PS might be ascribed to the negative effect of the 8T tail and the weak interaction between PS and FBS proteins. In contrast, the covalent bonding aptamer 6C3-7SF gave an IC_{50} of 15.2 ± 3.6 nM (0.27 ± 0.06 μg/mL), more than 25-fold and 100-fold enhancement over its noncovalent counterparts 6C3 and 6C3-7PS, respectively, showing the benefit of the covalent inhibition mechanism. The successful enhancement of pseudovirus neutralization by 6C3-7SF in DMEM containing 10% FBS also confirmed the sufficient specificity of 6C3-7SF to RBD/Spike in a complicated biological medium containing serum proteins. Under fluorescence microscope, the cells infected by 6C3-7SF-treated pseudoviruses displayed GFP fluorescence before lysis (Figure 4d) in the similar trend as the luciferase assy after lysis (Figure 4c). We observed no 293T cytotoxicity from 6C3-7SF even up to 1 μM (Figure 4e).

The SuFEx modification strategy we showed here should be compatible with the well-known aptamer multimerization strategy,[9-15] because luckily the innocent oligonucleotides as the linkers between the aptamer motifs in the multimers can be modified with PS and thus SF to provide the covalent inhibition mechanisms. Combining the two strategies is anticipated to give highly efficient virus neutralizers, though resulting in multimer inhibitors of larger molecular sizes. It should be noted that our method in the current form is still compromised by the use of PS tail modifications at the end of the aptamers, which can reduce the pseudovirus neutralization efficacy as shown in the case of 6C3-7PS versus 6C3 (Figure 4c). The 6C3-7SF synthesized

based on 6C3-7PS actually enhanced the pseudovirus neutralization for > 100-fold over 6C3-7PS, indicating the covalent bonding mechanism itself is highly efficient in improving the inhibition activities. However, this enhancement ratio of 6C3-7SF is lowered to only > 25-fold over 6C3 due to the reduced activity of 6C3-7PS. We expect that the exact structures of RBD-aptamer complexes, though not availabe yet, will help the rational design of more robust covalent bonding inhibitors against RBD-ACE2 and the virus infection.

Conclusion

In summary, we developed an efficient covalent bonding aptamer for RBD-ACE2 blocking and SARS-CoV-2 pseudovirus neutralization by modifying a known RBD aptamer with multiple SuFEx modifications. This chemically modified aptamer, 6C3-7SF, underwent strong covalent bonding with RBD at the important amino acid residues within the RBD-ACE2 binding interface. The covalent reactivity between 6C3-7SF and RBD was highly selective over ACE2 and serum proteins. Stronger RBD-ACE2 blocking and more effective SARS-CoV-2 pseudovirus neutralization were both observed for 6C3-7SF over the original aptamer 6C3, indicating the advantage of introducing the covalent inhibition mechanism. We believe that, like peptides and proteins,[28-31] many aptamers can also be converted into efficient covalent inhibitors of PPIs to offer inhibition with higher potency and longer duration, and the SuFEx-modified aptamers described in this work for covalent inhibition of RBD-ACE2 is just one example of this promising field.

Experimental Section

Materials

Chemicals for buffers and polyacrylamide gels were from either Sigma Aldrich (Shanghai, China), Alfa Aesar (Tianjin, China) or Solarbio (Beijing, China). Reagents for chemical reactions, including 4-(bromomethyl)benzenesulfonyl fluoride (Br-SF), p-toluenesulfonyl fluoride, DL-dithiothreitol (DTT), N-

ethylmaleimide, sodium hydroxide, 1-butanol and acetonitrile were purchased from Sigma Aldrich (Shanghai, China). Human ACE2 (Cat# 10108-H02H), SARS-CoV-2 spike protein (Cat# 40591-V08H), Fc-tag RBD (Cat# 40150-V05H), His-tag RBD (Cat# 40150-V08B2), His-tag RBD-N501Y (Cat# 40592-V08H82) and mouse monoclonal SARS-CoV-2 neutralizing antibody (Cat# 40592-MM57) were from Sino Biological (Beijing, China). We also purchased His-tag RBD (Cat# SPD-C52H2) and His-tag RBD-R408I (Cat# SPD-S52H8) from Acro Biosystems (Beijing, China). Human serum albumin (HSA) and human serum were from Sigma Aldrich (Shanghai, China). Human IgG1 Fc (FCC-H5214) was from Acro Biosystems (Beijing, China). Sequencing grade trypsin (Cat# V5113) was from Promega (Beijing, China). Amicon Ultra centrifugal filters (Amicon-10K) were from Merck KGaA (Darmstadt, Germany). The SARS-CoV-2 inhibitor screening kit (Cat# EP-105) and ELISA reagent set (Cat# EBS-001) were from Acro Biosystems (Beijing, China). Dulbecco's modified Eagle's medium (DMEM), fetal bovine serum (FBS), 100 IU/mL penicillin-streptomycin and 0.25% trypsin were purchased from Corning Cellgro (NY, USA). 293T cells stably expressing ACE2 and the SARS-CoV-2 pseudoviruses with CMV-GFP-IRES-Luciferase vectors (Cat# FNV215) were from Fubio (Shanghai, China). SARS-CoV-2 pseudoviruses (Cat# PSV001) with only luciferase vectors were purchased from Sino Biological (Beijing, China) and used to confirm the similar neutralization capability of the covalent bonding aptamer. All the oligonucleotides were purchased from Integrated DNA Technologies (IA, USA), Genscript (Jiangsu, China) or Hippobio (Zhejiang, China), with the sequences shown in Table S1 in Supporting Information. ESI-MS analyses of DNAs were through the commercial service provided by Sangon Biotech (Shanghai, China) or Genscript (Beijing, China), where we submitted 10 μL frozen samples of 50-100 μM DNA water solutions.

Synthesis of SF-modified aptamers

SF-modified aptamers were prepared by reacting Br-SF with PS-containing aptamers shown in Table S1. To a 50 μL solution of 100 μM PS-containing aptamers in 100 mM sodium phosphate buffer at pH 6.0 was

added 50 μL 30 mM Br-SF in CH_3CN. The solution was kept at 37 °C for 12-24 h. The resulting solution was combined with 200 μL water and extracted by 200 μL 1-butanol twice. The bottom (water) phase was purified by Amicon-10K ultrafilters using water for 6 times. The concentration of the final SF-modified aptamer solution was quantified by the standard UV260 method, and the stock solution was diluted to desired concentrations for other experiments. Denatured polyacrylamide gel electrophoresis (PAGE) and ESI-MS were used to characterize the SF-modified aptamer products. Upon storage at −20 °C, the SF-modified aptamer products were found stable in stock solution for at least 1 months (avoid freeze-thaw cycles).

Denatured PAGE analysis of aptamers before and after reactions

For the data shown in Figure 1b, aptamer samples dissolved in 1×PBS were mixed with 2-fold volume of 8 M urea, and were electrophoresed at 200 V for around 1 h on 10% denatured polyacrylamide gels (29:1 monomer to bis ratio, 8 M urea) in 1×TBE running buffer (90 mM Tris, 90 mM boric acid, 2 mM Na_2EDTA, pH 8.3) using the vertical electrophoretic apparatus (DYY-6C, Liuyi Instrument Factory, Beijing, China). After Thermofisher SYBR Gold (1×) staining, the gels were visualized using a Biorad Gel Doc XR+ Gel Documentation System.

For the data shown in Figure 2g, 1 μM aptamers (6C3-7SF or 6C3-7PS) were reacted with 1 μM proteins in 1×PBS containing 2 mM $MgCl_2$ for 2 h or indicated time at 37 °C. Then the solutions were mixed with 2-fold volume of 8 M urea and analysed by 10% denatured PAGE using the same condition as above.

SDS-PAGE analysis of proteins before and after reactions

For the SDS-PAGE data shown in Figure 2, 1 μM proteins were reacted with 1.5 μM aptamers in 1×PBS containing 2 mM $MgCl_2$ for 2 h or indicated time at 37 °C. Then the solution was mixed with 1/5 volume of 6× Loading Buffer (1×: 50 mM Tris, 2% SDS, 0.1% bromophenol blue, 10% glycerol) and heated at 90 °C for 1 min, followed by electrophoresis at 160 V for around 1 h on 8% SDS PAGE in 1× Running Buffer (25 mM Tris, 200 mM glycine, 1% mM SDS, pH 8.3). After stained by Instant Blue (Sigma Aldrich) or One-step Blue

(Biotium), the gels were imaged by a typical scanner or the Biorad Gel Doc XR+ Gel Documentation System. The reaction rate was calculated using ImageJ software based on the SDS-PAGE gel images in Figure 2h to give the chart in Figure 2i.

For Cy3-6C3-7SF reacting with RBD in diluted serum, 100 nM DNA and 400 nM protein were used (data shown in Figure S1b). Fluorescence imaging (Cy3 channel) was carried out for SDS-PAGE gels without protein stain, in the Biorad Gel Doc XR+ Gel Documentation System.

LC-MS/MS analysis for covalent bonding site identification

The RBD-6C3-7SF adducts were formed by reacting 1.5 μM 6C3-7SF with 1 μM RBD in 400 μL 1×PBS containing 2 mM $MgCl_2$ for 2 h at 37 ºC. The solution was desalted by Amicon-10K ultrafilters using water for 6 times, then added with NaOH to reach 0.1 M and allowed to react for 0.5 h at 25 ºC to remove the DNA parts from the RBD-6C3-7SF adducts. The resulting solution was desalted by Amicon-10K ultrafilters using water for 6 times and concentrated by Amicon-10K to about 25 μL, which was further added to 200 μL solution containing 2 mM DTT, 8 M urea, 50 mM Tris-HCl pH 8.3 and kept for 1 h at 37 ºC to break the RBD disulfide bonds. Then, N-ethylmaleimide was added to the solution to 10 mM and allowed a further reaction for 1 h at 37 ºC to alkylate thiols from both cysteines and SF-modified residues. The solution was subsequently desalted by Amicon-10K ultrafilters using 25 mM Tris-HCl pH 8.3 for 6 times and concentrated by Amicon-10K to about 25 μL. In solution digestion was performed by adding trypsin into the sample at a 1: 50 ratio (w/w, trypsin:protein) and incubating overnight at room temperature. The final solution was acidified and cleaned up using C18 spin columns before LC-MS/MS analysis. Peptides were first separated by UltiMate3000 RSLCnano ultra high performance liquid chromatography (UHPLC) system, and then analyzed by a Thermo Scientific Orbitrap Eclipse Tribrid mass spectrometer equipped with electron transfer dissociation (ETD) functionality at Tsinghua University. Collected MS/MS spectra were searched by Proteome Discoverer 2.4 software, and then manually inspected for verification of peptide sequences and

modification sites.

As a negative control, 400 μL 1 μM RBD was treated using the same protocol as above to confirm no SF-modified residue was detected in the peptide fragmentation signals for the protein alone. For *p*-toluenesulfonyl fluoride reaction, 5 mM *p*-toluenesulfonyl fluoride was used instead of 1.5 μM 6C3-7SF, and all the other steps were the same as above.

RBD-ACE blocking activity assay using ELISA

Coating Step: In the high-bind 96-well plates, 2.5 ng/μL RBD (around 100 nM) or its variant in 100 μL Coating Buffer (15 mM Na_2CO_3, 35 mM $NaHCO_3$, pH 9.6) was added to each well except for the blank wells (no RBD). The plates were covered by tape and kept for 2 h at 37 ºC.

Blocking Step: After washing each well by 300 μL Washing Buffer (1× PBS, pH 7.4, 0.05% Tween-20) for three times, the plates were blocked by adding 300 μL Blocking Buffer (2% BSA, 1× PBS, pH 7.4) to each well. The plates were covered by tape and kept for 1 h at 37 ºC.

Reacting Step: After washing each well by 300 μL Reacting Buffer (1× PBS, 2 mM $MgCl_2$, pH 7.4) for three times, aptamer samples in 100 μL Reacting Buffer were added to each well. Negative and positive controls were 100 μL Reacting Buffer and 500 nM kit-included inhibitor (ACE2) in 100 μL Reacting Buffer, respectively. The plates were covered by tape and kept for 2 h at 37 ºC.

Binding Step: After washing each well by 300 μL Washing Buffer for three times, 0.12 ng/μL biotinylated ACE2 in 100 μL Washing Buffer was added to each well. The plates were covered by tape and kept for 0.5 h at 37 ºC.

Labeling Step: After washing each well by 300 μL Washing Buffer for three times, 0.1 ng/μL Streptavidin-HRP in 100 μL Washing Buffer was added to each well. The plates were covered by tape and kept for 0.5 h at 37 ºC.

Testing Step: After washing each well by 300 μL Washing Buffer for three times, 100 μL substrate

solution from the kit (ELISA reagent set, Cat# EBS-001, Acro Biosystems) was added to each well. Blue color generation was observed from the HRP-active wells. After about 20 min of enzymatic reaction, 50 μL stop solution from the kit was added to each well and the blue color turned yellow. The plates were read at 450 nm using a UV/Vis microplate spectrophotometer.

For all the above tests, each sample was repeated at least three times in one set of experiment.

SARS-CoV-2 pseudovirus neutralization activity assay

293T cells stably expressing ACE2 were cultured in 96-well plates (~10,000 cells seeded per well) in 100 μL DMEM with 10% FBS. The cells were ready for pseudovirus infection after about 20 h when reaching ~70% confluence.

Serial dilutions of each aptamer (0.0256-2000 nM) or antibody (0.0018-28 μg/mL) in 100 μL DMEM containing 10% FBS and 3 mM Mg^{2+} were pre-incubated with 5 μL 10^8~10^9 copies/mL pseudoviruses in microtubes for 2.5 h at 37 °C, and then the mixtures were added to ACE2-expressing 293T cells cultured in 96-well plates to reach 200 μL per well. After 6 h infection, the culture medium was refreshed to 100 μL DMEM containing 10% FBS, and then cells were cultured at 37 °C for another 48 h. After that, 100 μL One-Lumi reagent from the RG055 kit of Beyontime (Shanghai, China) was added to each well to initiate cell lysis and supply the luciferase substrate. After reaction at room temperature for 5 min, the luciferase activity was measured on a Multimode Microplate Reader (Tecan Spark). Fluorescence images were taken on an Olympus FV-1200 confocal laser scanning microscope (Tokyo, Japan).

For cell viability analysis, 0 or 500 or 1000 nM PEG-6C3-7SF was added to each wells of ACE2-expressing 293T cells. After 48 h incubation at 37 °C, cell viability was assessed using the enhanced CCK-8 kit from Beyotime (Shanghai, China). The absorbance was read at 450 nm by a microplate reader.

All the experiments involving 293T cells or SARS-CoV-2 pseudoviruses were carried out in a BSL-2 laboratory.

Acknowledgements

This work is supported by the National Key Research and Development Program of China (No.2021YFA1200900) and the National Natural Science Foundation of China (Nos. 21621003 and 22074076). We thank Ms. Mingyun Wang from Boston College for the help in manuscript proofreading. The figures in this paper were prepared using the Biorender tools and templates, with the full approval of publication licenses.

References

1. Lan, J.; Ge, J.; Yu, J.; Shan, S.; Zhou, H.; Fan, S.; Zhang, Q.; Shi, X.; Wang, Q.; Zhang, L.; Wang, X., Structure of the SARS-CoV-2 spike receptor-binding domain bound to the ACE2 receptor. *Nature* **2020,** *581*, 215-220.

2. Shang, J.; Ye, G.; Shi, K.; Wan, Y. S.; Luo, C. M.; Aihara, H.; Geng, Q. B.; Auerbach, A.; Li, F., Structural basis of receptor recognition by SARS-CoV-2. *Nature* **2020,** *581*, 221-224.

3. Guo, Y.; Huang, L.; Zhang, G.; Yao, Y.; Zhou, H.; Shen, S.; Shen, B.; Li, B.; Li, X.; Zhang, Q.; Chen, M.; Chen, D.; Wu, J.; Fu, D.; Zeng, X.; Feng, M.; Pi, C.; Wang, Y.; Zhou, X.; Lu, M.; Li, Y.; Fang, Y.; Lu, Y. Y.; Hu, X.; Wang, S.; Zhang, W.; Gao, G.; Adrian, F.; Wang, Q.; Yu, F.; Peng, Y.; Gabibov, A. G.; Min, J.; Wang, Y.; Huang, H.; Stepanov, A.; Zhang, W.; Cai, Y.; Liu, J.; Yuan, Z.; Zhang, C.; Lou, Z.; Deng, F.; Zhang, H.; Shan, C.; Schweizer, L.; Sun, K.; Rao, Z., A SARS-CoV-2 neutralizing antibody with extensive spike binding coverage and modified for optimal therapeutic outcomes. *Nat. Commun.* **2021,** *12*, 2623.

4. Jones, B. E.; Brown-Augsburger, P. L.; Corbett, K. S.; Westendorf, K.; Davies, J.; Cujec, T. P.; Wiethoff, C. M.; Blackbourne, J. L.; Heinz, B. A.; Foster, D.; Higgs, R. E.; Balasubramaniam, D.; Wang, L.; Zhang, Y.; Yang, E. S.; Bidshahri, R.; Kraft, L.; Hwang, Y.; Zentelis, S.; Jepson, K. R.; Goya, R.; Smith, M. A.; Collins, D. W.; Hinshaw, S. J.; Tycho, S. A.; Pellacani, D.; Xiang, P.; Muthuraman, K.; Sobhanifar, S.; Piper, M. H.; Triana, F. J.; Hendle, J.; Pustilnik, A.; Adams, A. C.; Berens, S. J.; Baric, R. S.; Martinez, D. R.; Cross, R. W.; Geisbert, T. W.; Borisevich, V.; Abiona, O.; Belli, H. M.; de Vries, M.; Mohamed, A.; Dittmann, M.; Samanovic, M. I.; Mulligan, M. J.; Goldsmith, J. A.; Hsieh, C. L.; Johnson, N. V.; Wrapp, D.; McLellan, J. S.; Barnhart, B. C.; Graham, B. S.; Mascola, J. R.; Hansen, C. L.; Falconer, E., The neutralizing antibody, LY-CoV555, protects against SARS-CoV-2 infection in nonhuman primates. *Sci. Transl. Med.* **2021,** *13*, eabf1906.

5. Bojadzic, D.; Alcazar, O.; Chen, J.; Chuang, S. T.; Condor Capcha, J. M.; Shehadeh, L. A.; Buchwald, P., Small-molecule inhibitors of the coronavirus spike: ACE2 protein-protein interaction as blockers of viral attachment and entry for SARS-CoV-2. *ACS Infect. Dis.* **2021,** *7*, 1519-1534.

6. Toelzer, C.; Gupta, K.; Yadav, S. K. N.; Borucu, U.; Davidson, A. D.; Williamson, M. K.; Shoemark, D. K.; Garzoni, F.; Staufer, O.; Milligan, R.; Capin, J.; Mulholland, A. J.; Spatz, J.; Fitzgerald, D.; Berger, I.; Schaffitzel, C., Free fatty acid binding pocket in the locked structure of SARS-CoV-2 spike protein. *Science* **2020,** *370*, 725-730.

7. Schutz, D.; Ruiz-Blanco, Y. B.; Munch, J.; Kirchhoff, F.; Sanchez-Garcia, E.; Muller, J. A., Peptide and peptide-based inhibitors of SARS-CoV-2 entry. *Adv. Drug Deliv. Rev.* **2020,** *167*, 47-65.

8. Larue, R. C.; Xing, E. M.; Kenney, A. D.; Zhang, Y. X.; Tuazon, J. A.; Li, J. R.; Yount, J. S.; Li, P. K.; Sharma, A., Rationally designed ACE2-derived peptides inhibit SARS-CoV-2. *Bioconjug. Chem.* **2021,** *32*, 215-223.

9. Sun, M.; Liu, S.; Wei, X.; Wan, S.; Huang, M.; Song, T.; Lu, Y.; Weng, X.; Lin, Z.; Chen, H.; Song, Y.; Yang, C., Aptamer

blocking strategy inhibits SARS-CoV-2 virus infection. *Angew. Chem. Int. Ed.* **2021,** *60*, 10266-10272.
10. Liu, X.; Wang, Y. L.; Wu, J.; Qi, J.; Zeng, Z.; Wan, Q.; Chen, Z.; Manandhar, P.; Cavener, V. S.; Boyle, N. R.; Fu, X.; Salazar, E.; Kuchipudi, S. V.; Kapur, V.; Zhang, X.; Umetani, M.; Sen, M.; Willson, R. C.; Chen, S. H.; Zu, Y., Neutralizing aptamers block S/RBD-ACE2 interactions and prevent host cell infection. *Angew. Chem. Int. Ed.* **2021,** *60*, 10273-10278.
11. Kacherovsky, N.; Yang, L. F.; Dang, H. V.; Cheng, E. L.; Cardle, I. I.; Walls, A. C.; McCallum, M.; Sellers, D. L.; DiMaio, F.; Salipante, S. J.; Corti, D.; Veesler, D.; Pun, S. H., Discovery and characterization of spike n-terminal domain-binding aptamers for rapid SARS-CoV-2 detection. *Angew. Chem. Int. Ed.* **2021,** *60*, 21211-21215.
12. Peinetti, A. S.; Lake, R. J.; Cong, W.; Cooper, L.; Wu, Y.; Ma, Y.; Pawel, G. T.; Toimil-Molares, M. E.; Trautmann, C.; Rong, L.; Marinas, B.; Azzaroni, O.; Lu, Y., Direct detection of human adenovirus or SARS-CoV-2 with ability to inform infectivity using DNA aptamer-nanopore sensors. *Science Advances* **2021,** *7*.
13. Schmitz, A.; Weber, A.; Bayin, M.; Breuers, S.; Fieberg, V.; Famulok, M.; Mayer, G., A SARS-CoV-2 spike binding DNA aptamer that inhibits pseudovirus infection by an RBD-independent mechanism**. *Angew. Chem. Int. Ed.* **2021,** *60*, 10279-10285.
14. Valero, J.; Civit, L.; Dupont, D. M.; Selnihhin, D.; Reinert, L. S.; Idorn, M.; Israels, B. A.; Bednarz, A. M.; Bus, C.; Asbach, B.; Peterhoff, D.; Pedersen, F. S.; Birkedal, V.; Wagner, R.; Paludan, S. R.; Kjems, J., A serum-stable RNA aptamer specific for SARS-CoV-2 neutralizes viral entry. *Proc. Natl. Acad. Sci. U. S. A.* **2021,** *118*.
15. Zhang, Z.; Pandey, R.; Li, J.; Gu, J.; White, D.; Stacey, H. D.; Ang, J. C.; Steinberg, C.-J.; Capretta, A.; Filipe, C. D. M.; Mossman, K.; Balion, C.; Miller, M. S.; Salena, B. J.; Yamamura, D.; Soleymani, L.; Brennan, J. D.; Li, Y., High-affinity dimeric aptamers enable the rapid electrochemical detection of wild-type and b.1.1.7 SARS-CoV-2 in unprocessed saliva. *Angew. Chem. Int. Ed.* **2021,** *60*, 24266-24274.
16. Singh, J.; Petter, R. C.; Baillie, T. A.; Whitty, A., The resurgence of covalent drugs. *Nat. Rev. Drug Discovery* **2011,** *10*, 307-317.
17. Lagoutte, R.; Patouret, R.; Winssinger, N., Covalent inhibitors: An opportunity for rational target selectivity. *Curr. Opin. Chem. Biol.* **2017,** *39*, 54-63.
18. Lonsdale, R.; Ward, R. A., Structure-based design of targeted covalent inhibitors. *Chem. Soc. Rev.* **2018,** *47*, 3816-3830.
19. Zhang, T. H.; Hatcher, J. M.; Teng, M. X.; Gray, N. S.; Kostic, M., Recent advances in selective and irreversible covalent ligand development and validation. *Cell Chem. Biol.* **2019,** *26*, 1486-1500.
20. Mukherjee, H.; Grimster, N. P., Beyond cysteine: Recent developments in the area of targeted covalent inhibition. *Curr. Opin. Chem. Biol.* **2018,** *44*, 30-38.
21. Moore, A. R.; Rosenberg, S. C.; McCormick, F.; Malek, S., Ras-targeted therapies: Is the undruggable drugged? *Nat. Rev. Drug Discovery* **2020,** *19*, 533-552.
22. Abdeldayem, A.; Raouf, Y. S.; Constantinescu, S. N.; Moriggl, R.; Gunning, P. T., Advances in covalent kinase inhibitors. *Chem. Soc. Rev.* **2020,** *49*, 2617-2687.
23. Dai, W.; Zhang, B.; Jiang, X. M.; Su, H.; Li, J.; Zhao, Y.; Xie, X.; Jin, Z.; Peng, J.; Liu, F.; Li, C.; Li, Y.; Bai, F.; Wang, H.; Cheng, X.; Cen, X.; Hu, S.; Yang, X.; Wang, J.; Liu, X.; Xiao, G.; Jiang, H.; Rao, Z.; Zhang, L. K.; Xu, Y.; Yang, H.; Liu, H., Structure-based design of antiviral drug candidates targeting the SARS-CoV-2 main protease. *Science* **2020,** *368*, 1331-1335.
24. Karges, J.; Kalaj, M.; Gembicky, M.; Cohen, S. M., Re-I tricarbonyl complexes as coordinate covalent inhibitors for the SARS-CoV-2 main cysteine protease. *Angew. Chem. Int. Ed.* **2021,** *60*, 10716-10723.
25. Chaikuad, A.; Koch, P.; Laufer, S. A.; Knapp, S., The cysteinome of protein kinases as a target in drug development. *Angew. Chem. Int. Ed.* **2018,** *57*, 4372-4385.
26. Pettinger, J.; Jones, K.; Cheeseman, M. D., Lysine-targeting covalent inhibitors. *Angew. Chem. Int. Ed.* **2017,** *56*, 15200-15209.
27. Ueda, T.; Tamura, T.; Kawano, M.; Shiono, K.; Hobor, F.; Wilson, A. J.; Hamachi, I., Enhanced suppression of a protein-protein interaction in cells using small-molecule covalent inhibitors based on an n-acyl-n-alkyl sulfonamide warhead. *J. Am. Chem. Soc.* **2021,** *143*, 4766-4774.
28. Gambini, L.; Baggio, C.; Udompholkul, P.; Jossart, J.; Salem, A. F.; Perry, J. J. P.; Pellecchia, M., Covalent inhibitors of protein-protein interactions targeting lysine, tyrosine, or histidine residues. *J. Med. Chem.* **2019,** *62*, 5616-5627.
29. Gambini, L.; Udompholkul, P.; Baggio, C.; Muralidharan, A.; Kenjic, N.; Assar, Z.; Perry, J. J. P.; Pellecchia, M., Design,

synthesis, and structural characterization of lysine covalent BH3 peptides targeting Mcl-1. *J. Med. Chem.* **2021,** *64*, 4903-4912.
30. Li, Q. K.; Chen, Q.; Klauser, P. C.; Li, M. Y.; Zheng, F.; Wang, N. X.; Li, X. Y.; Zhang, Q. B.; Fu, X. M.; Wang, Q.; Xu, Y.; Wang, L., Developing covalent protein drugs via proximity-enabled reactive therapeutics. *Cell* **2020,** *182*, 85-97.
31. Berdan, V. Y.; Klauser, P. C.; Wang, L., Covalent peptides and proteins for therapeutics. *Bioorg. Med. Chem.* **2021,** *29*, 115896.
32. Dong, J. J.; Krasnova, L.; Finn, M. G.; Sharpless, K. B., Sulfur(VI) fluoride exchange (SuFEx): Another good reaction for click chemistry. *Angew. Chem. Int. Ed.* **2014,** *53*, 9430-9448.
33. Narayanan, A.; Jones, L. H., Sulfonyl fluorides as privileged warheads in chemical biology. *Chem. Sci.* **2015,** *6*, 2650-2659.
34. Martin-Gago, P.; Olsen, C. A., Arylfluorosulfate-based electrophiles for covalent protein labeling: A new addition to the arsenal. *Angew. Chem. Int. Ed.* **2019,** *58*, 957-966.
35. Brighty, G. J.; Botham, R. C.; Li, S. H.; Nelson, L.; Mortenson, D. E.; Li, G. C.; Morisseau, C.; Wang, H.; Hammock, B. D.; Sharpless, K. B.; Kelly, J. W., Using sulfuramidimidoyl fluorides that undergo sulfur(vi) fluoride exchange for inverse drug discovery. *Nat. Chem.* **2020,** *12*, 906-913.
36. Maurais, A. J.; Weerapana, E., Reactive-cysteine profiling for drug discovery. *Curr. Opin. Chem. Biol.* **2019,** *50*, 29-36.
37. Tabuchi, Y.; Yang, J.; Taki, M., Inhibition of thrombin activity by a covalent-binding aptamer and reversal by the complementary strand antidote. *Chem. Commun.* **2021,** *57*, 2483-2486.
38. Tivon, Y.; Falcone, G.; Deiters, A., Protein labeling and crosslinking by covalent aptamers. *Angew. Chem. Int. Ed.* **2021,** *60*, 15899-15904.
39. Xiao, L.; Gu, C.; Xiang, Y., Orthogonal activation of RNA-cleaving dnazymes in live cells by reactive oxygen species. *Angew. Chem. Int. Ed.* **2019,** *58*, 14167-14172.
40. Gu, C. M.; Xiao, L.; Shang, J. C.; Xu, X.; He, L.; Xiang, Y., Chemical synthesis of stimuli-responsive guide RNA for conditional control of CRISPR-Cas9 gene editing. *Chem. Sci.* **2021,** *12*, 9934-9945.
41. Antonysamy, S.; Bonday, Z.; Campbell, R. M.; Doyle, B.; Druzina, Z.; Gheyi, T.; Han, B.; Jungheim, L. N.; Qian, Y. W.; Rauch, C.; Russell, M.; Sauder, J. M.; Wasserman, S. R.; Weichert, K.; Willard, F. S.; Zhang, A. P.; Emtage, S., Crystal structure of the human PRMT5:MEP50 complex. *Proc. Natl. Acad. Sci. U. S. A.* **2012,** *109*, 17960-17965.
42. Fu, W. Y.; Chen, Y. J. A.; Wang, K. D.; Hettinghouse, A.; Hu, W. H.; Wang, J. Q.; Lei, Z. N.; Chen, Z. S.; Stapleford, K. A.; Liu, C. J., Repurposing FDA-approved drugs for SARS-CoV-2 through an ELISA-based screening for the inhibition of RBD/ACE2 interaction. *Protein Cell* **2021,** *12*, 586-591.